Hindawi Publishing Corporation
EURASIP Journal on Advances in Signal Processing
Volume 2010, Article ID 380473, 15 pages
doi:10.1155/2010/380473

Research Article

Artificial Neural Network-Based Clutter Reduction Systems for Ship Size Estimation in Maritime Radars

R. Vicen-Bueno, R. Carrasco-Álvarez, M. Rosa-Zurera (EURASIP Member), J. C. Nieto-Borge, and M. P. Jarabo-Amores

Signal Theory and Communications Department, Superior Politechnic School, University of Alcalá, Alcalá de Henares, 28805 Madrid, Spain

Correspondence should be addressed to R. Vicen-Bueno, raul.vicen@uah.es

Received 1 July 2009; Revised 16 November 2009; Accepted 14 January 2010

Academic Editor: Frank Ehlers

The existence of clutter in maritime radars deteriorates the estimation of some physical parameters of the objects detected over the sea surface. For that reason, maritime radars should incorporate efficient clutter reduction techniques. Due to the intrinsic nonlinear dynamic of sea clutter, nonlinear signal processing is needed, what can be achieved by artificial neural networks (ANNs). In this paper, an estimation of the ship size using an ANN-based clutter reduction system followed by a fixed threshold is proposed. High clutter reduction rates are achieved using 1-dimensional (horizontal or vertical) integration modes, although inaccurate ship width estimations are achieved. These estimations are improved using a 2-dimensional (rhombus) integration mode. The proposed system is compared with a CA-CFAR system, denoting a great performance improvement and a great robustness against changes in sea clutter conditions and ship parameters, independently of the direction of movement of the ocean waves and ships.

1. Introduction

The measurement of physical parameters of the sea surface by radar systems plays an important role in ocean surveillance and remote sensing. Depending on the application, two different points of view can be identified. From the first one, sea measurements contain useful information about the ocean surface. The characterization of the nonlinear dynamic of sea waves becomes the focal point of the study. From the second one, if the primary objective is the detection of objects over the sea surface, such as ships and/or boats, and the posterior estimation of their physical parameters, the information about the sea surface is referred as sea clutter and viewed as an interference to suppress. The studies presented in this paper are focused on the last case, where the separation of sea clutter and ship information allows the estimation of ship physical parameters.

Maritime radar systems usually only measure the intensity of the returned electromagnetic echo (incoherent measurement). This kind of systems is commonly used, for instance, in maritime traffic control centers. They are considered to estimate some ship physical parameters in our studies. Among other final applications, one part of our proposal, the clutter reduction system (CRS), could improve the information managed by automatic identification systems (AISs) [1], such as the detection, positioning, and tracking of surrounding ships, which lets improve the safety of maritime navigation.

An analysis of different clutter reduction techniques can be found in [2, 3]. They can be divided, among others, in three categories: based on image processing; based on statistical signal processing and constant false alarm rate (CFAR) systems; and based on artificial neural networks (ANNs), which are relatively novel. As explained below, all these techniques denote that linear signal processing cannot be applied. First, because the dynamic of sea clutter is intrinsically nonlinear. And second, because the target (ship/s) and clutter (waves) spectra can be overlapped because of their spectral distributions and their relative movement (Doppler effect). These reasons indicate that nonlinear signal processing is needed.

Among all the possibilities of the techniques based on image processing, we focus on those that use transformed domains. Clutter reduction in radar images by using a translation invariant wavelet packet decomposition is proposed in [4, 5]. On the other hand, the information contained in temporal radar image sequences captured by a WaMoS II system (see Section 2.1) is used in [6, 7]. These works use the Fourier transform to estimate certain parameters of the ocean waves. This technique is also used in [8] to filter sea clutter and detect ships in movement based on the acquired experience about their spectra. However, these solutions usually make the system working slowly (high computational cost and memory requirements) and presents the information with some delay, what we try to avoid in our proposal.

The techniques based on statistical signal processing usually suppose an statistical model known a priori (Weibull-distributed, k-distributed, etc.) for the clutter. In this case, an approach to reduce ground clutter is proposed in [9], where a simple parametric model is used, what limits its application to other kinds of clutter, such as sea clutter. The estimation of target and clutter signal parameters by the use of likelihood-ratio-tests is considered in [10] to reduce the level of clutter in surface penetrating impulse radars. Other approaches based on statistical signal processing, such as independent and principal component analyses, were also successfully applied in [11, 12], respectively. On the other hand, the techniques based on CFAR systems are commonly used in radar signal processing. Cell averaging CFAR (CA-CFAR) systems [13, 14] are used in automatic radar detection, where CA is used previous to detection. Other techniques could be used, such as the ones based on order statistics [15] or distributed CFAR processing [16], but the commonly used CA-based system is taken as a reference in our studies.

The last category of techniques is based on ANNs. These techniques do not need the a priori knowledge of the target and clutter statistical distributions and their parameters, as required by some statistical methods. These techniques only need some preclassified input data. But, why does it happen? Because the ANNs are able to learn during training some statistical properties of input data. The use of ANNs, such as the radial basis function (RBF) ANNs, denotes the suitable applicability of these techniques in clutter reduction to detect radar targets [17, 18]. Other kinds of ANNs, such as the feedforward multilayer perceptrons (MLPs), are used to approximate the Neyman-Pearson detector [19]. Moreover, they are also applied in [20, 21] to nonlinearly reduce sea clutter in maritime radars when the information from a radar image is selected in a 1-dimensional (1D) mode (horizontally and vertically, resp.). Both algorithms were developed using a fixed number of integrated cells, but, what happens if a different number of integrated cells is used? Can the clutter reduction system be improved if 2-dimensional (2D) modes are used to select the information from the radar image? The answer to these questions are the key points of the system proposal presented in the current paper.

The paper is divided in several sections. Section 2 describes the instrumentation used to get the radar measurements and the composition of the database of radar images obtained from these measurements. The designing and testing stages of the proposed ANN-based clutter reduction system followed by a threshold are explained in Section 3, where a special attention is paid to the 2D integration mode considered in our studies. The performance achieved with the proposed system is presented in Section 4, where a study of the optimum number of integrated cells in 1D and 2D modes when using the ANN and CA-based approaches is done. Moreover, subjective and objective analyses of a specific radar image are done using both approaches, paying special attention to the obtained ship size estimations. Finally, Section 5 presents the main conclusions and contributions of our study.

Table 1: Transmission and reception characteristics of the maritime radar system.

Radar system frequency (X-band)	10.0	GHz
Antenna polarization	H and H	
Antenna rotation Speed	6.4	rpm
Pulse repetition frequency (PRF)	1000	Hz
Radar pulse width	80	ns
Azimuthal range (Coverage)	0–360	°
Azimuthal resolution	0.28	°
Distance range (Coverage)		
Standard configuration	200–2150	m
Fast acquisition	150–1350	m
Range resolution	7.5	m

2. Measuring and Monitoring Maritime System: Database Composition

The measuring and monitoring maritime system used to obtain the electromagnetic measurements is described first. Thereafter, the radar images obtained from these measurements are grouped in different sets, composing the database used in our experiments.

2.1. Measuring and Monitoring Maritime System. The radar measurements considered in our experiments are obtained from the FINO 1 (Forschungsplattformen in Nord-und Ostsee) German research platform located in the North Sea. This platform incorporates a measuring and monitoring system [22], as shown in Figure 1. The standard technical configuration is given in Table 1, where a short coverage range is also used for fast data acquisition (the range resolution is maintained constant). Both coverage configurations are considered to achieve different radar images, which compose the database used in our studies.

This measurement system is based on an incoherent standard X-band maritime radar, that, among other properties, incorporates a logarithmic amplifier and has no frequency agility. The analog video signal in the radar unity display is digitized by the WaMoS II [23] Analog-to-Digital (A/D) converter. In the standard configuration of the system, a temporal sequence of 32 consecutive radar images every five minutes (antenna rotation period) is acquired. The

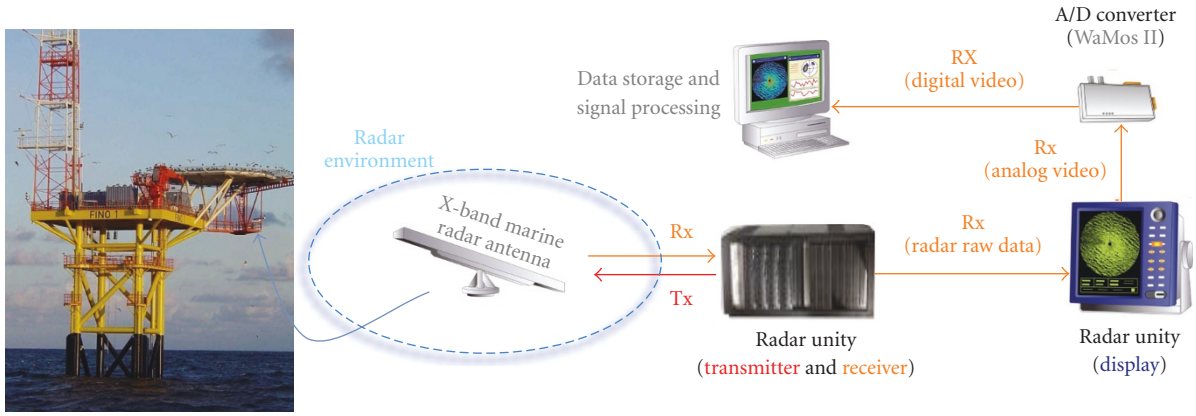

Figure 1: Measuring and monitoring maritime system.

image spatial resolution depends on the azimuthal and range resolutions of the system. The intensity of each radar image cell is coded without sign and 8 bits, what sets a cell dynamic range of [0–255]. Finally, the digitized images are processed by a standard computer to perform the desired radar application by software, such as the sea clutter reduction and ship size estimation presented in this paper. Note that, because of the radar raw data from the WaMoS II system are used, no signal preprocessing is done before the clutter reduction system is applied.

2.2. Database of Radar Images. The database selected for the experiments is composed of a set of 12 different sequences of radar images obtained by the radar measurement system presented above. All these sequences are different from each other to cover different sea states (height, period, and character/type of waves on the surface of a large body of water: deep water waves and spilling breakers) and types of ships. On one hand, sea states 1–5 of the World Meteorological Organization [24] are considered. On the other hand, different kinds of ships are considered: general cargo ships, ferries, container ships and cruise ships, with maximum widths of 31 m and maximum lengths of 281 m, approximately. Depending on the sea state and type and relative position of the ship present in the radar image, different Signal-to-Clutter Ratios (SCRs) are observed. In our case of study, for images containing information of sea state 1, average SCRs of 17 dB are observed. Whereas, for images containing information of sea state 5, average SCRs of 9 dB are observed.

One half of these 12 sequences represent a radar environment where a target (ship) is present in sea clutter. The other half represents situations where no target is present. Thus, this variability of sequences tries to cover the different possibilities where the radar can work.

According to the way the proposed ANN-based clutter reduction system is designed and tested (see Section 3.2), 8 radar image sequences are dedicated to design it: 4 to compose the training data set and 4 to compose the validation data set, whereas the remaining 4 sequences are dedicated to test the performance of the system once designed. On the other hand, taking into account that each image ($N \times N$ pixels) contains a total of 332,929 pixels ($N = 577$), where a maximum of 257,307 pixels are valid (360° coverage area), only several images from each sequence are selected because of the training speed of the used ANN. In this case, the different compositions and sizes of the sets are as follows [20]:

(i) *training set*: 4 representative images of the 4 sequences of the training data set (16 *images*),

(ii) *validation set*: 4 representative images of the 4 sequences of the validation data set (16 *images*),

(iii) *testing set*: 8 representative images of the 4 sequences of the testing data set (32 *images*).

According to the composition of the different sets, two important aspects are emphasized. First, the number of observation vectors obtained from the three sets (dimensionality of the sets) is enough to achieve high estimation accuracies in the designing and testing stages. And second, the test set is composed of target (ship) and clutter (sea states) conditions different from the ones used in the training and validation sets. It allows the designers to estimate the robustness of the designed system against changes in the environmental conditions of the radar.

3. Ship Size Estimation by ANN-Based Clutter Reduction Systems and Thresholding

In this section, the new mode to select the input data from a radar image is investigated to improve the ANN-based clutter reduction system performance. The ANN designing and testing stages are described. The way of evaluating its performance, its computational cost, and the procedure followed to obtain the optimum number of ANN inputs (integrated cells) are also presented.

3.1. ANN and CA-Based Approaches Using Different Input Data Integration Modes. The way the ANN-based clutter reduction and CA systems process the input radar image (**I**) is described below. Figure 2 shows the scheme of the

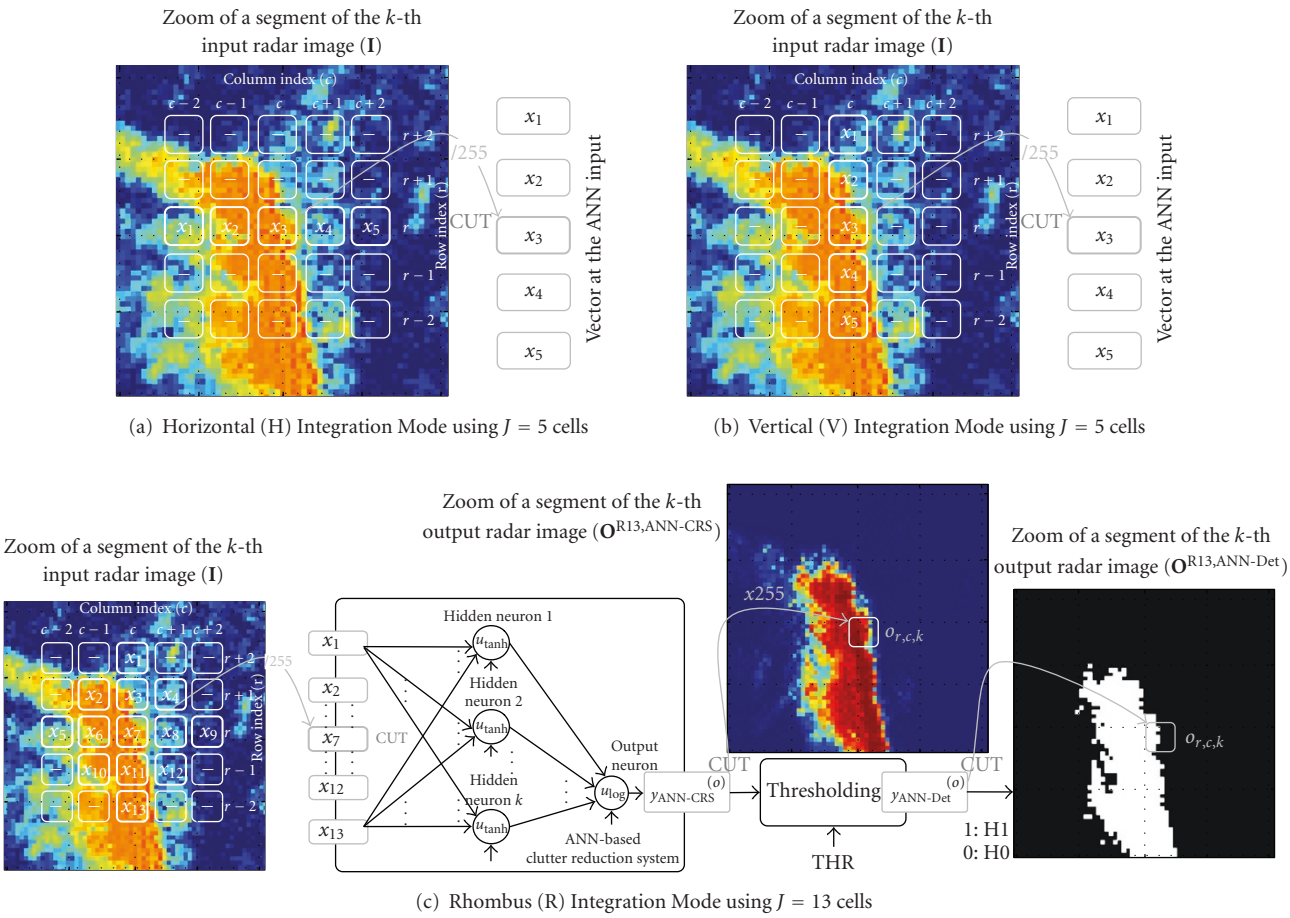

(a) Horizontal (H) Integration Mode using $J = 5$ cells

(b) Vertical (V) Integration Mode using $J = 5$ cells

(c) Rhombus (R) Integration Mode using $J = 13$ cells

FIGURE 2: H, V, and R integration modes considering an RIA = 5 cells in the detection system based on ANN-based clutter reduction system.

proposed system for an integration of 5 cells in 1D and 2D modes. So, different output radar images ($\mathbf{O}$) are obtained, being analyzed in Section 4.

The analysis of the works [20, 21], where a fixed number of measurements are selected in horizontal and vertical modes, respectively, provoked us the following question: why not to combine 1D modes to improve the clutter reduction system performance? In this case, a different way of working is proposed for clutter reduction systems: the rhombus (R) integration mode. This mode is based on the 2D Von Neumann neighborhood selection [25]. This integration mode is presented in Figure 2(c) for a range of integrated area (RIA) of 5 cells. Note that the selection of cells is done from a square of RIA × RIA cells. Another important parameter in our studies is the number of integrated cells (J) in the system, where J also denotes the number of ANN inputs. So, J = RIA in 1D modes, whereas they are different in the rhombus mode, being $J = (\text{RIA}-1)((\text{RIA}-1)/2+1)+1$ [25].

The way to obtain the output ($y^{(o)}$) of a general clutter reduction system for a cell under test (CUT) is shown in Figure 2, although this figure is particularized for the ANN-based system. The vector $\mathbf{x}$ at the input of the clutter reduction system, and its relationship with the original image is described in (1) for a vertical mode, being r and c the row and column indexes in the image, respectively, and k the index of the image in the set. J must be odd because the CUT is in the middle of $\mathbf{x}$.

$$\begin{aligned}\mathbf{x} &= [x_1 \cdots x_{J+1/2} \cdots x_J] \\ &= \left[\frac{i_{r+((\text{RIA}-1)/2),c,k}}{255} \cdots \frac{i_{r,c,k}}{255} \cdots \frac{i_{r-((\text{RIA}-1)/2),c,k}}{255}\right].\end{aligned} \tag{1}$$

The dynamic range of the input data (8 bits: [0 − 255]) is normalized to a range [0 − 1], and the output is in the range [0 − 1]. This output is finally denormalized to the same range as the input image for illustration purposes. According to the input vector given in (1), the output of the CA system is achieved as

$$y_{\text{CA}}^{(o)} = f_{\text{CA}}(x) = \frac{1}{J-1}\sum_{i=1}^{J} x_i, \quad i \neq \frac{J+1}{2}, \tag{2}$$

whereas the output of the CA-CFAR system [26] for a fixed threshold of THR = 0.5 is obtained as

$$y_{\text{CA-CFAR}}^{(o)} = \frac{x_{(J+1)/2}}{y_{\text{CA}}^{(o)}} \underset{\text{H}_0}{\overset{\text{H}_1}{\gtrless}} 0.5; \tag{3}$$

that is, $y_{\text{CA-CFAR}}^{(o)}$ is 1 or 0 if this division is greater or lower than THR, respectively.

On the other hand, the ANN output is computed as

$$y^{(o)}_{ANN-CRS} = f_{ANN}(\mathbf{x}), \tag{4}$$

where $f_{ANN}(\cdot)$ denotes the ANN transfer function, being nonlinear in our studies.

From here on, special attention is paid to the computation of the ANN output in two steps. A general ANN structure ($J/K/1$) composed of J inputs, K hidden neurons, and 1 output neuron is considered.

Consider that $\mathbf{v}^{(h)}$ is a vector of size $[1 \times K]$ that stores the addition of the weighted inputs of each hidden neuron. Also, consider that the vector $\mathbf{y}^{(h)}$ of size $[1 \times K]$ stores the outputs of each hidden neuron. And finally, consider $\mathbf{W}^{(h)}$ being a matrix of size $[J \times K]$ that contains the synaptic weights that connect the ANN inputs with the ANN hidden neurons and $\mathbf{b}^{(h)}$ is a row vector of size $[1 \times K]$ that contains the hidden neuron biases. According to $\mathbf{W}^{(h)}$ and $\mathbf{b}^{(h)}$, (5) shows how $\mathbf{v}^{(h)}$ is computed to finally obtain $\mathbf{y}^{(h)}$ by (6). Note that a *hyperbolic tangent* activation function ($\psi_{\tanh}(\cdot)$) [27] is used in this layer.

$$\mathbf{v}^{(h)} = \mathbf{x}\mathbf{W}^{(h)} + \mathbf{b}^{(h)}, \tag{5}$$

$$\mathbf{y}^{(h)} = \psi_{\tanh}\left(\mathbf{v}^{(h)}\right) = \frac{\sinh\left(\mathbf{v}^{(h)}\right)}{\cosh(\mathbf{v}^{(h)})} = \frac{e^{\mathbf{v}^{(h)}} - e^{-\mathbf{v}^{(h)}}}{e^{\mathbf{v}^{(h)}} + e^{-\mathbf{v}^{(h)}}}. \tag{6}$$

Now consider that $v^{(o)}$ is a variable that contains the addition of the weighted inputs to the output neuron, as presented in (7). Moreover, consider that $\mathbf{w}^{(o)}$ is a column vector of size $[K \times 1]$ that contains the connection weights between the hidden neuron outputs and the output neuron input, and $b^{(o)}$ denotes the bias of the output neuron. Finally, the neuron output ($y^{(o)}_{ANN-CRS}$) is computed by (8). Note that because the ANN output is in the range $[0 - 1]$, this neuron uses a *logistic* activation function ($\psi_{\log}(\cdot)$).

$$v^{(o)} = \mathbf{y}^{(h)}\mathbf{w}^{(o)} + b^{(o)}, \tag{7}$$

$$y^{(o)}_{ANN-CRS} = \psi_{\log}\left(v^{(o)}\right) = \frac{1}{1 + e^{v^{(o)}}}. \tag{8}$$

Finally, the output of the ANN-based detection system for a fixed threshold of THR = 0.5 is achieved by (9), being 1 or 0 if it is greater or lower than THR, respectively,

$$y^{(o)}_{ANN-Det} = y^{(o)}_{ANN-CRS} \underset{H_0}{\overset{H_1}{\gtrless}} 0.5. \tag{9}$$

3.2. Designing and Testing Stages of the ANN. As described in the previous section, the ANN output for a certain CUT is obtained by (5)–(8). An estimation of how good the achieved ANN output is needed during the designing process. This estimation is done by the mean squares (MS) error [19] (cost function to minimize) in its nth iteration as

$$e_{MS}[n] = \frac{1}{MNN}\sum_{k=1}^{M}\sum_{r=1}^{N}\sum_{c=1}^{N}\frac{\left(d_{r,c,k}/255 - o_{r,c,k}[n]/255\right)^2}{2}, \tag{10}$$

where $d_{r,c,k}$ and $o_{r,c,k}$ denote the elements placed at the rth row and cth column of the kth desired ($\mathbf{D}$) and obtained ($\mathbf{O}$) ANN output images of the set, respectively. N is the size of one dimension of the squared radar images and M is the number of radar images in the set.

In our studies, the learning algorithm based on error back-propagation with adaptive learning rate and momentum is applied, as used in [20, 21]. This learning algorithm automatically updates the weights and biases of the ANN for the following algorithm iteration $(n + 1)$. Moreover, an off-line actualization of the weights and biases and an external validation [28] of the training process are carried out.

As observed, the error estimation carried out in the training process needs the desired output (desired radar image). It can be a problem in real-life situations due to the difficulty of obtaining these ideal images. To solve this difficulty, two procedures can be used, among others. In the first one, using the information provided by AIS data (type of ship: length and width) and knowing the central position and orientation of the ship, the ideal image could be generated to estimate the performance of the proposed system in practically real-time. But, as the AIS data is not available in our experiments, the procedure followed in [20] to obtain the desired radar images for a given sequence of radar images is selected. But, note that once the system is designed and working in steady state, the knowledge of the desired image is not mandatory to visually analyze the obtained radar images. Nevertheless, the desired images are also generated in the testing stage to report objective measurements of the system performance.

Once the desired outputs are determined and the training algorithm is set, the ANN-based clutter reduction system is designed. The designing procedure [20] is summarized in four steps: a driven initialization of 10 MLPs of size $J/K/1$ is chosen; a set of training algorithm parameters that warrants its stability and convergence [28] is used; an external validation of the training process is applied; and a selection of the best MLP in terms of average SCR improvements is done.

Finally, once the system is designed, its performance is objectively evaluated by using a set of radar images never applied during the designing stage, the testing set.

3.3. Objective Performance Evaluation: Clutter Reduction, Ship Size and Computational Cost Estimations. The performance evaluation of a clutter reduction system can be done by comparing the input and output radar images. This comparison presents problems because subjective interpretation is done. This is the reason why several objective measurements are used in our studies, apart from the MS error used in the ANN training. Note that for the objective measurements presented below, the knowledge of the desired output radar images is needed. The designer could think that these measurements of the performance could not be done, but once the system is designed and working in steady state, these measurements could be estimated if a detector is applied to discern whether target is present or not in the CUTs. These objective measurements are calculated for a given radar image and for a set of them [20].

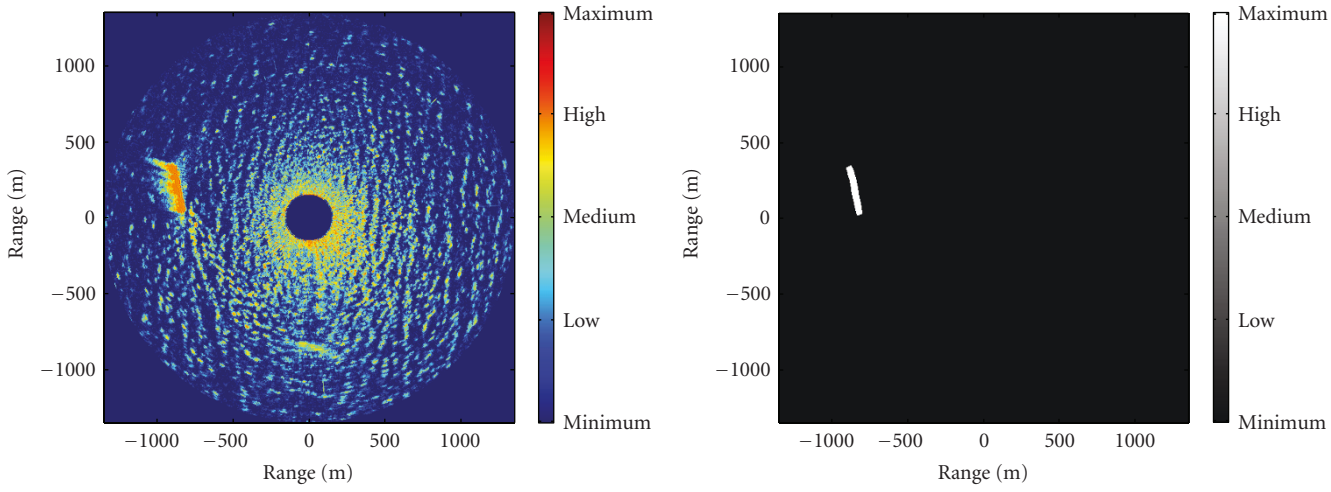

(a) Input (**I**) (b) Desired Output (**D**)

Figure 3: Input Radar Image Containing Target (Ship) in Sea Clutter and its Desired System Output.

Table 2: Performance evaluation ($SCR^{\text{av,imp}}$ (dB)) of CA- and ANN-based clutter reduction systems with different number of integrated cells, J, considering 1D integration modes.

		ANN-based Clutter Reduction System						CA-based System					
RIA	ANN struct.	*Horizontal mode*			*Vertical mode*			*Horizontal mode*			*Vertical mode*		
(cells)	(J/10/1)	Train	Val.	Test	Train	Val.	Test	Train	Val.	Test	Train	Val.	Test
3	03/10/1	9.9	9.7	9.6	9.6	9.5	9.2	0.4	0.4	0.4	0.5	0.5	0.5
5	05/10/1	12.5	12.4	12.1	11.5	11.3	11.1	0.6	0.6	0.6	0.7	0.7	0.7
7	07/10/1	12.6	12.5	12.2	12.2	12.0	11.7	0.9	0.9	0.9	1.1	1.1	1.1
9	09/10/1	12.7	12.7	12.4	12.6	12.6	12.3	1.2	1.2	1.2	1.2	1.2	1.2
11	11/10/1	12.8	12.7	12.4	12.6	12.5	12.3	1.2	1.2	1.2	1.2	1.2	1.2
13	13/10/1	12.6	12.5	12.2	12.6	12.4	12.3	1.1	1.1	1.1	1.1	1.1	1.1
15	15/10/1	12.3	12.1	11.8	12.6	12.4	12.2	0.8	0.8	0.8	0.9	0.9	0.9
17	17/10/1	12.0	11.9	11.7	12.4	12.2	12.0	0.8	0.8	0.8	0.9	0.9	0.9
19	19/10/1	11.5	11.5	11.2	12.1	12.0	11.6	0.7	0.7	0.7	0.8	0.8	0.8

On one hand, the objective measurements considered for a given radar image are as follows.

(i) Consider the target and clutter powers at the system input, P_{t}^{in} (dBm) and P_{c}^{in} (dBm), and output, $P_{\text{t}}^{\text{out}}$ (dBm) and $P_{\text{c}}^{\text{out}}$ (dBm). The estimations of each powers are done considering the CUTs where target is present and absent, respectively. Then, the target and clutter power improvements are

$$\begin{aligned} \text{P}_t^{\text{imp}}\,(\text{dB}) &= P_{\text{t}}^{\text{out}} - P_{\text{t}}^{\text{in}}\,, \\ \text{P}_c^{\text{imp}}\,(\text{dB}) &= P_{\text{c}}^{\text{out}} - P_{\text{c}}^{\text{in}}\,. \end{aligned} \tag{11}$$

(ii) The Signal-to-Clutter Ratio improvement is obtained as

$$\begin{aligned} \text{SCR}^{\text{imp}}\,(\text{dB}) &= \text{SCR}^{\text{out}}\,(\text{dB}) - \text{SCR}^{\text{in}}\,(\text{dB}) \\ &= \left[P_{\text{t}}^{\text{out}} - P_{\text{c}}^{\text{out}}\right] - \left[P_{\text{t}}^{\text{in}} - P_{\text{c}}^{\text{in}}\right] \\ &= \text{P}_t^{\text{imp}} - \text{P}_c^{\text{imp}}. \end{aligned} \tag{12}$$

On the other hand, the objective measurements used for a given set of M radar images are as follows:

(i) the average P_{t} and P_{c} improvements, denoted as $P_{\text{t}}^{\text{av,imp}}$ and $P_{\text{c}}^{\text{av,imp}}$, respectively,

(ii) the average SCR improvement:

$$\text{SCR}^{\text{av,imp}}\,(\text{dB}) = \frac{1}{M}\sum_{i=1}^{M}\text{SCR}_i^{\text{imp}}\,(\text{dB}). \tag{13}$$

The estimation of the performance of the clutter reduction systems is very important in the overall system, because the greater the achieved $\text{SCR}^{\text{av,imp}}$, the more accurate the ship size estimation, as shown in the results (see Section 4). The estimation of the ship size is based on the positioning of a rectangle in the radar image obtained after thresholding. The length of the sides of this rectangle indicates the estimated width (short side) and length (long side) of a ship. The positioning of the rectangle is done by finding a huge area

Table 3: Performance evaluation of CA- and ANN-based clutter reduction systems with different number of integrated cells, J, considering a 2D (rhombus (R)) integration mode.

		ANN-based Clutter Reduction System									CA-based System		
RIA	ANN struct.	$P_c^{av,imp}$ (dB)			$P_t^{av,imp}$ (dB)			$SCR^{av,imp}$ (dB)			$SCR^{av,imp}$ (dB)		
(cells)	(RJ/10/1)	Train	Val.	Test	Train	Val.	Test	Train	Val.	Test	Train	Val.	Test
3	R05/10/1	−11.3	−10.1	−10.0	1.3	1.3	1.1	11.6	11.4	11.1	0.6	0.6	0.6
5	R13/10/1	−13.1	−12.9	−12.8	1.4	1.4	1.1	14.5	14.3	13.9	1.1	1.1	1.1
7	**R**25/10/1	−15.6	−15.3	−15.2	1.6	1.6	1.4	17.2	16.9	16.6	1.4	1.4	1.4
9	**R**41/10/1	−16.4	−16.0	−15.8	1.7	1.7	1.5	18.1	17.7	17.3	1.4	1.4	1.4
11	R61/10/1	−16.3	−15.7	−15.6	1.7	1.7	1.5	17.8	17.4	17.1	1.3	1.3	1.3
13	R85/10/1	−15.6	−15.2	−15.1	1.8	1.8	1.5	17.4	17.0	16.6	1.2	1.2	1.2
15	R113/10/1	−15.2	−14.8	−14.7	1.9	1.9	1.6	17.1	16.7	16.3	1.0	1.0	1.0
17	R145/10/1	−13.9	−13.7	−13.5	1.8	1.8	1.5	15.7	15.4	15.1	0.9	0.9	0.9
19	R181/10/1	−13.6	−13.4	−13.2	1.8	1.8	1.5	15.4	15.1	14.8	0.8	0.8	0.8

of points that surpassed the fixed threshold. In this case, the proposed system is designed to work correctly when medium and huge ship sizes are present in the radar coverage area. These sizes are typical for ships that travel on the open sea.

Another important parameter of the system is the computational cost. Equation (14) gives the number of memory cells needed to store the ANN synaptic weights, products, and two-element sums necessary to process each CUT by the ANN.

$$\begin{aligned} &\text{Memory Cells}: \ (J+1)\cdot K + (K+1)\cdot 1, \\ &\text{Products}: \ J\cdot K + K\cdot 1, \\ &\text{Sums}: \ J\cdot K + K\cdot 1. \end{aligned} \tag{14}$$

3.4. Determination of the Best Number of Integrated Cells and Range of Integrated Area. The range of integrated area, RIA, and consequently the number of integrated cells (ANN inputs), J, are important parameters in the proposed system. The procedure to evaluate their optimum values is based on the objective performance evaluation ($SCR^{av,imp}$) of the clutter reduction system in the designing stage. For this study, an ANN with $K = 10$ hidden neurons is selected, being an appropriate value to obtain high clutter reduction rates, as discussed in [20, 21]. Following the designing procedure presented in Section 3.2 for $K = 10$ and for different values of J, the best ANN structure is selected in terms of the highest $SCR^{av,imp}$ achieved with the validation set.

4. Results: System Configuration for Ship Size Estimations

This section presents the performances (SCR improvements and ship size estimations) achieved by the CA-CFAR system (reference system) and the ANN-based clutter reduction system with a fixed threshold when the different integration modes under study are used. First, a study of the optimum range of integrated area and number of integrated cells in the systems is done for each integration mode. In the next stage, subjective and objective analyses of the results obtained for a radar image are discussed. Finally, the ship size estimations for the different systems and configurations are presented.

Table 4: Performance improvements achieved by the CA and ANN-based clutter reduction systems for the radar image under study of Figure 3.

	ANN-based Clut. Red. Sys		*CA-based System*	
	Performance	Figure	Performance	Figure
	Horizontal / Vertical (09/10/1)		*Horizontal / Vertical* ($J = 9$)	
P_c^{imp}	−8.3/−8.7		−1.0 / −1.2	
P_t^{imp}	+2.1/+2.0	4(a)/4(b)	−0.3 / −0.0	6(a)/6(b)
SCR^{imp}	+10.4/+10.7		+0.7 / +1.2	
	Rhombus (R41/10/1)		*Rhombus* ($J = 7$)	
P_c^{imp}	−12.4		−1.1	
P_t^{imp}	+2.3	4(c)	−0.1	6(c)
SCR^{imp}	+14.7		+1.0	

4.1. Integration Modes: Best RIA and Number of Integrated Cells (J) in Clutter Reduction Systems. A study of the optimum RIA and number of integrated cells, J, is presented in this section for 1D and 2D integration modes when both the ANN-based clutter reduction and CA-CFAR systems are considered. Moreover, a computational cost analysis is also given for each mode in the ANN-based approach.

4.1.1. 1-D Integration Modes. Horizontal (H) and Vertical (V). A study of the optimum values of RIA and J using the horizontal and vertical integration modes is given in Table 2.

After analyzing the results obtained with the validation set (designing stage), an increase of the average SCR improvement is observed until the optimum number of integrated cells is achieved (J = RIA = 9 cells). The average SCR improvements achieved, once the system is designed (testing stage), are slightly above 12 dB. These improvements are obtained by an average clutter power reduction slightly above 11 dB and an average target power enhancement above 1 dB. Moreover, greater values of J (15, 17, and 19 cells)

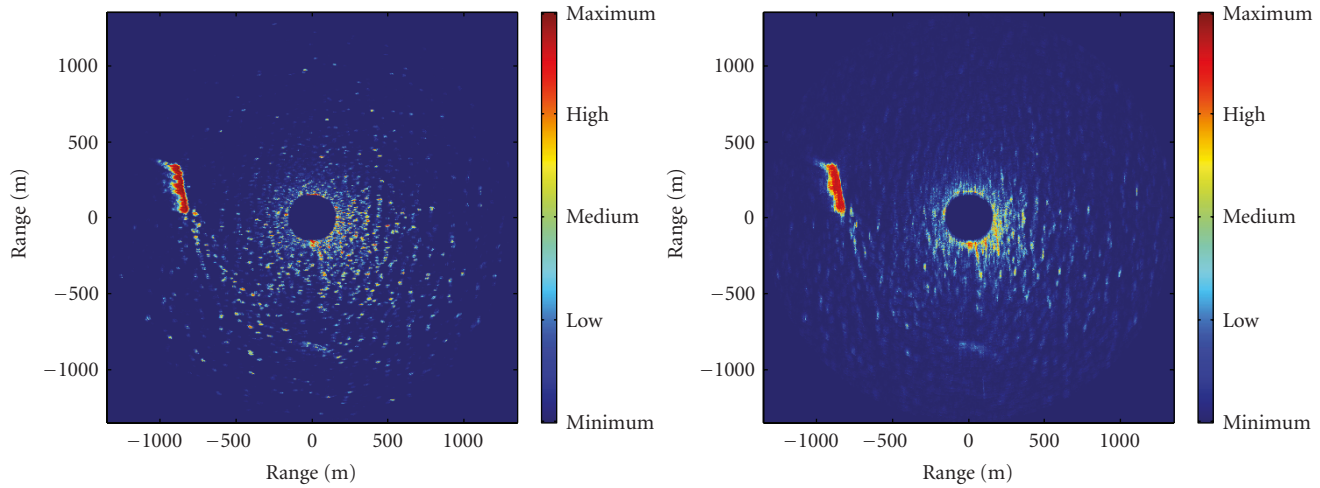

(a) Horizontal ANN-based CRS Output ($\mathbf{O}^{\text{H09,ANN-CRS}}$)

(b) Vertical ANN-based CRS Output ($\mathbf{O}^{\text{V09,ANN-CRS}}$)

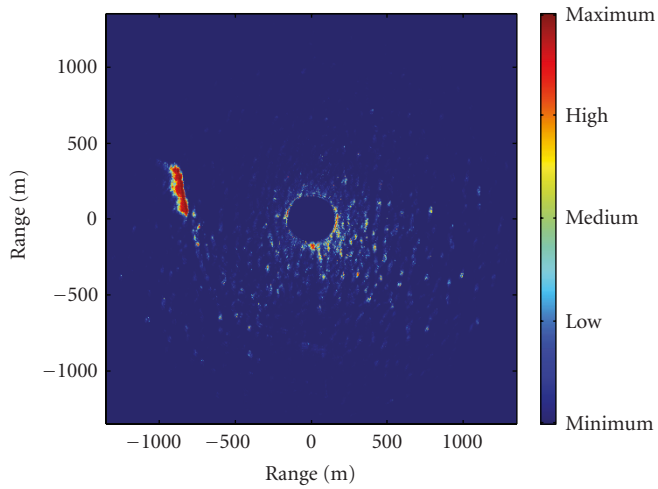

(c) Rhombus ANN-based CRS Output ($\mathbf{O}^{\text{R41,ANN-CRS}}$)

Figure 4: Radar Images Processed by the ANN-based Clutter Reduction System Using its Best H, V, and R Integration Modes.

not only do not warrant an increase of the performance improvement but also increase the performance loss.

On the other hand, considering the designing sets, the performances achieved by the ANN-based approach are always greater than the one of the testing set for a given J. It is usual behavior of the ANNs, because of the learning process. Nevertheless, note that the performances achieved with the testing and designing sets are very similar. In this case, their average SCR improvements only differ by 0.3 dB for the optimum case. This effect indicates that the training was correctly done and the system presents a great robustness against changes in the environmental conditions (designing and testing sets are different).

Focus now on the analysis of the results obtained with the system taken as reference, the CA-based approach. Its performance is always lower than the one obtained with the proposed system for any number of integrated cells. In this case, the optimum configuration is also RIA = J = 9 cells.

Finally, note that the system performances are very similar with both integration modes due to the circular symmetry of the radar coverage. The observed marginal differences are due to the random relative positions that the ships can take with respect to the radar site.

4.1.2. 2D Integration Mode. Rhombus (R). The performances of the systems which use the rhombus integration mode are presented in Table 3. As observed, the best performance in the ANN-based approach is achieved when RIA = 9 cells, that is, J = 41 inputs in the ANN. In this case, the average SCR improvement is greater than the ones obtained when 1D modes are used. The average SCR improvement is slightly above 17 dB once designed (testing stage), reducing and increasing the clutter and target average powers in around 16 and 1 dB, respectively.

Once again, the correct training and the great robustness of the designed ANN-based clutter reduction system with

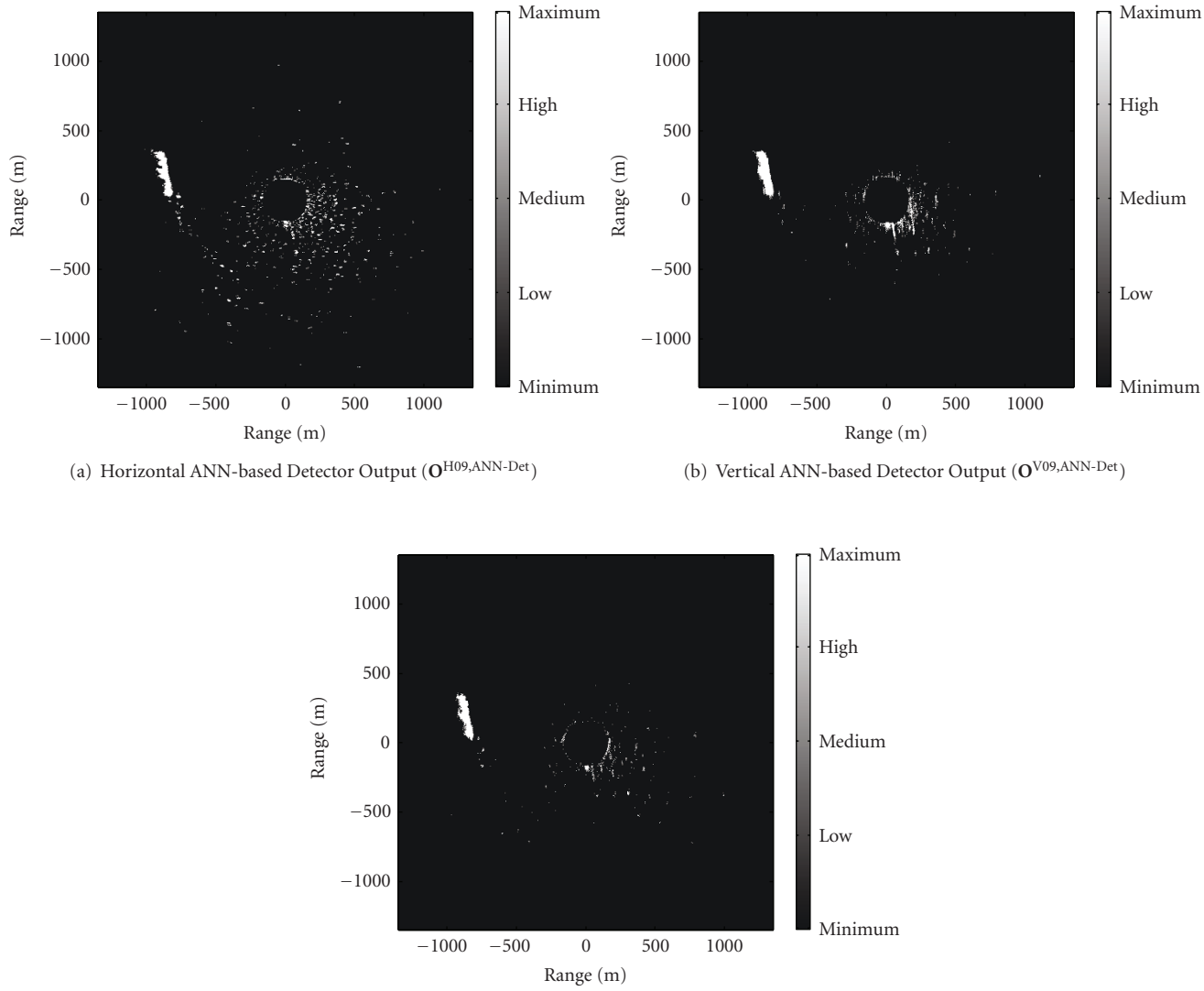

(a) Horizontal ANN-based Detector Output ($\mathbf{O}^{\text{H09,ANN-Det}}$)

(b) Vertical ANN-based Detector Output ($\mathbf{O}^{\text{V09,ANN-Det}}$)

(c) Rhombus ANN-based Detector Output ($\mathbf{O}^{\text{R41,ANN-Det}}$)

Figure 5: Radar Images Processed by the ANN-based Detection System Using its Best H, V, and R Integration Modes.

respect to changes in the radar environmental conditions (sea clutter and ship conditions vary in time) is demonstrated. In this case, the difference between the average SCR improvements for the designing and testing sets (maximum $\text{SCR}^{\text{av,imp}}$ loss of 0.8 dB) is greater than when 1D modes are used, although it is still a great robustness.

On the other hand, a different behavior is observed for the CA-based system. The best performance is for RIA = [7, 9] cells. In this case, RIA = 7 cells (J = 25 cells) are used because of the computational cost reduction. Nevertheless, although the performances are greater than the ones obtained when 1D modes are used, they are always lower than the ones obtained with the proposed system.

Once the optimum RIA and J values are selected for each integration mode, the computational cost of the ANN using each one is studied. In this case, the number of memory cells, products, and sums needed to process each CUT of a radar image (see (14)) are as follows:

(i) best case in the 1D modes (09/10/1): 111 memory cells, 100 products, and 100 sums,

(ii) best case in the rhombus (2D) mode (R41/10/1): 431 memory cells, 420 products, and 420 sums.

As observed, the computational cost of the proposed system using the rhombus (2D) integration mode is approximately four times the computational cost needed when 1D modes are used.

4.2. Integration Modes: Subjective and Objective Analyses of Processed Radar Images. Once the optimum number of integrated cells is found for each integration mode in CA- and ANN-based clutter reduction systems, a subjective analysis of their performances is carried out. In this case, a

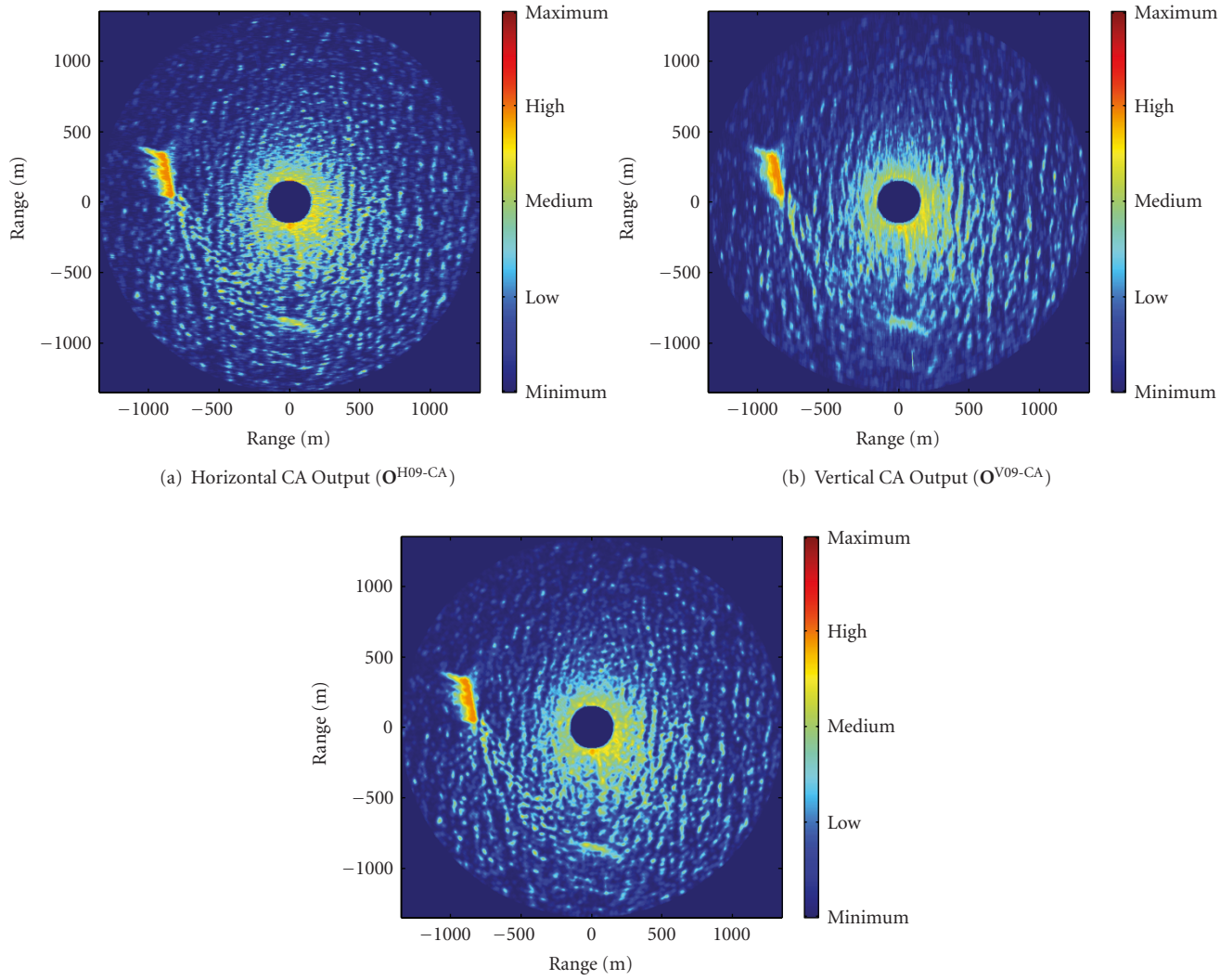

(a) Horizontal CA Output ($\mathbf{O}^{\text{H09-CA}}$)

(b) Vertical CA Output ($\mathbf{O}^{\text{V09-CA}}$)

(c) Rhombus CA Output ($\mathbf{O}^{\text{R25-CA}}$)

Figure 6: Radar Images Processed by the CA System Using its Best H, V, and R Integration Modes.

radar image containing a ship in sea clutter is selected from the testing set (see Figure 3(a)). It is important to note that there is only one ship (object of interest) in this radar image. The object located in the position [0 m, −900 m] is not of interest in our studies. It is a maritime research platform. For this image, the worst SCR improvement and ship size estimation of the images of the testing set has been found. For illustration purposes, the desired radar image at the output of the systems is presented in Figure 3(b).

The analysis of the performances of the ANN-based clutter reduction systems is done first. In this case, the best trained ANNs are selected for the following integration modes and structures: vertical 9/10/1, horizontal 9/10/1, and rhombus 41/10/1. The processed radar images are depicted in Figures 4 and 5. Next, the analysis of each case is carried out.

Using the 1D modes in the ANN-based approach with $J = 9$ integrated cells (see Figures 4(a) and 4(b)), the clutter power is highly reduced in areas far away from the radar site. Nevertheless, it is slightly reduced in areas near the radar site, where high remanent clutter power is still present. On the other hand, the target power is enhanced, also emphasizing the received electromagnetic diffraction produced in the unseen side of the ship, what makes the ship detection and shape definition more difficult. In this case, the output radar images of Figures 5(a) and 5(b) are obtained after thresholding (THR = 0.5). As observed, several false alarms are obtained where the remanent clutter power is still high. The cells where the ship is present are correctly detected. Nevertheless, the ship electromagnetic diffraction is also detected, generating several problems in the final estimation of the ship size, as discussed in Section 4.3. Finally, note that a difference is appreciated when horizontal and vertical modes are used. This difference is related to the way the remanent clutter power is distributed in the processed radar image, specially near the radar site. Whereas in the vertical mode the remanent clutter power is highly concentrated near the radar site, in the horizontal mode this remanent power could

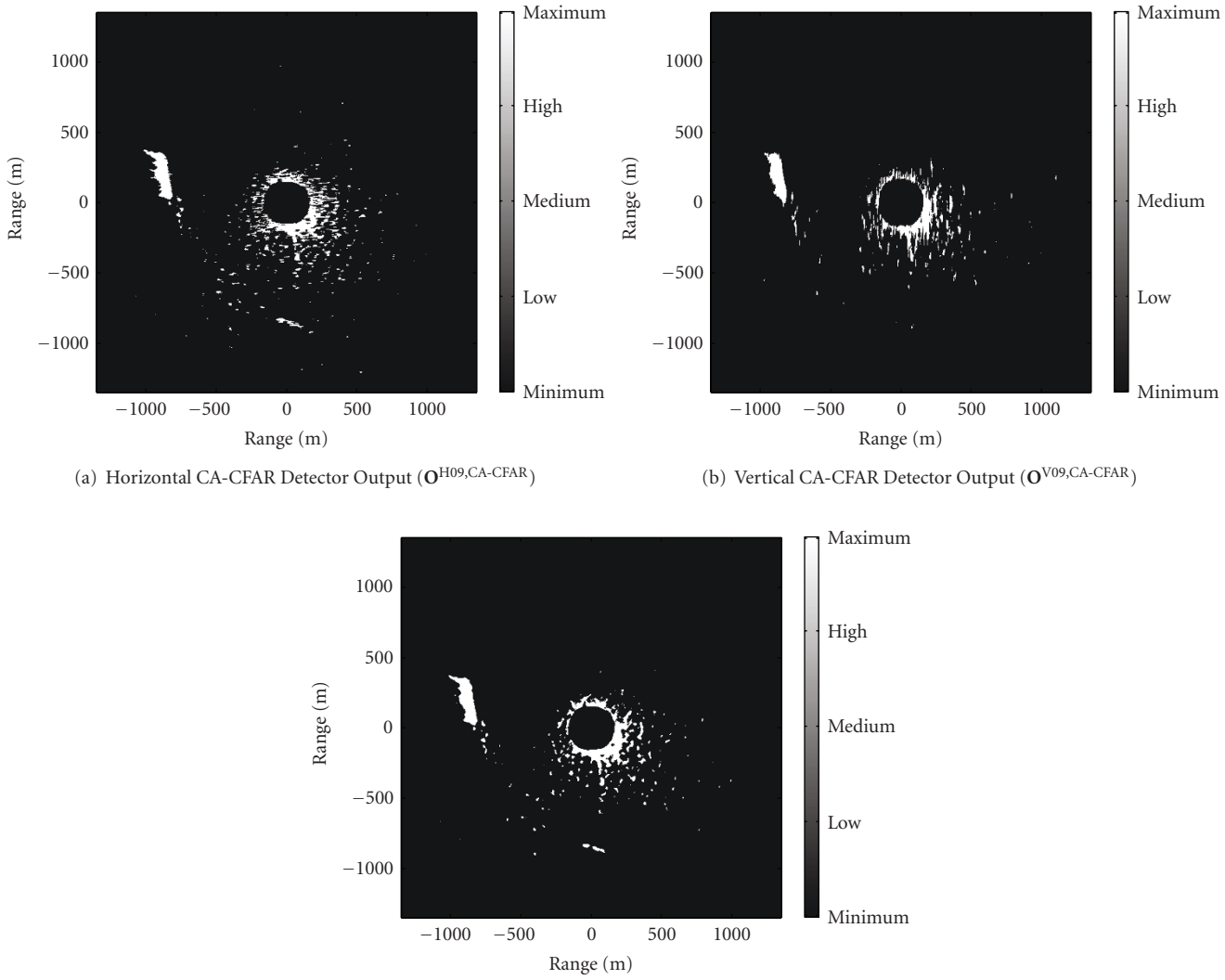

(a) Horizontal CA-CFAR Detector Output ($\mathbf{O}^{\text{H09,CA-CFAR}}$)

(b) Vertical CA-CFAR Detector Output ($\mathbf{O}^{\text{V09,CA-CFAR}}$)

(c) Rhombus CA-CFAR Detector Output ($\mathbf{O}^{\text{R25,CA-CFAR}}$)

Figure 7: Radar Images Processed by the CA-CFAR Detection System Using its Best H, V, and R Integration Modes.

be considered like a grainy and spread remanent clutter. This effect is due to the wave field propagating from right to left in the radar image.

Using a 2D mode (rhombus mode) in the ANN-based approach with $J = 41$ integrated cells (Figure 4(c)), better subjective performances than using 1D modes are achieved. In this case, the remanent clutter power is distributed in a different way, presenting few spikes of high clutter power instead of a uniformly distributed clutter power. On the other hand, the ship electromagnetic diffraction is more reduced now. So, a more accurate estimation of the ship size could be done (compare Figure 4(c) with Figure 3(b)). After thresholding (THR = 0.5), the output radar image of Figure 5(c) is obtained. As observed, the number of false alarms due to the clutter and the ship electromagnetic diffraction is reduced.

Next, the results obtained when applying the CA-CFAR system are presented for the different integration modes under study. Figures 6 and 7 show the radar images obtained after applying a cell averaging and thresholding, respectively. As observed in Figure 6, lower performances are achieved, independently of the integration mode, because neither the clutter power is substantially reduced nor the target power is enhanced. This low performance is due to the linear signal processing (cell averaging) applied. But, clutter reduction is not the aim of a CA-CFAR system. The aim is to detect cells of the radar coverage where ship information is present. From the subjective analysis of Figure 7, two problems are found. First, the huge areas where a target is absent (near the radar site) are incorrectly detected, generating confusion when a rectangle must be placed in the image. Second, the electromagnetic ship diffraction is still present and detected, generating problems in the ship size estimation, as discussed in Section 4.3.

Finally, an analysis of performance with objective measurements for the previous radar images is presented in Table 4. The best performance is achieved when the rhombus integration mode is used in the ANN-based

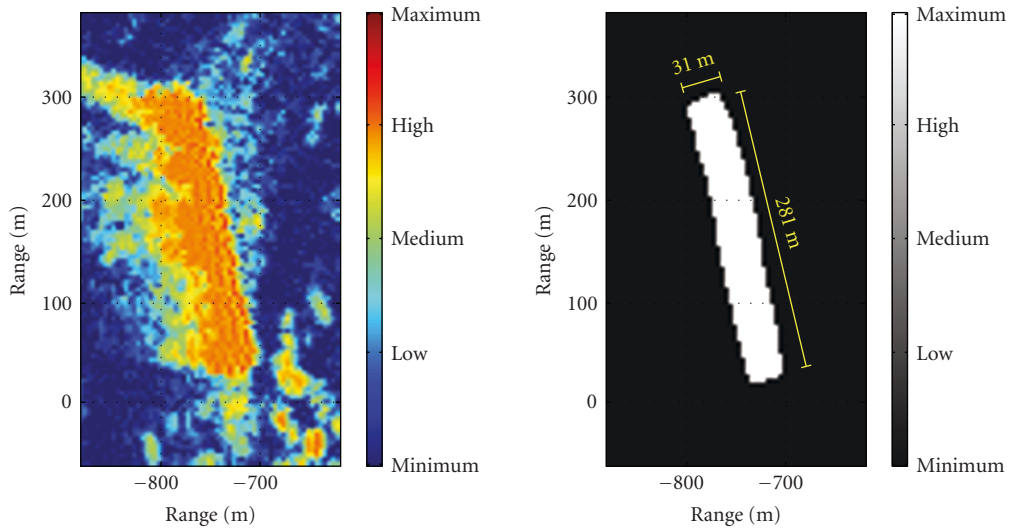

(a) Zoom of the Input (**I**) (b) Zoom of the Desired Output (**D**)

Figure 8: Zoom of the relevant area of the input (**I**) and desired output (**D**) Radar images of Figure 3.

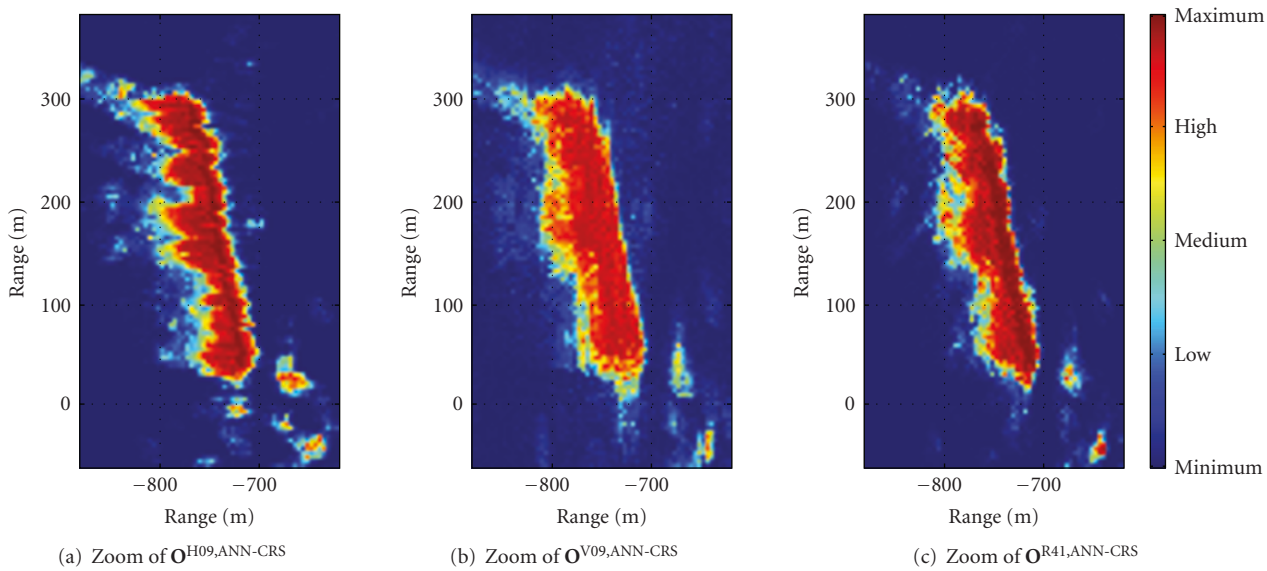

(a) Zoom of $\mathbf{O}^{\mathrm{H09,ANN\text{-}CRS}}$ (b) Zoom of $\mathbf{O}^{\mathrm{V09,ANN\text{-}CRS}}$ (c) Zoom of $\mathbf{O}^{\mathrm{R41,ANN\text{-}CRS}}$

Figure 9: Zoom of the Images Processed by the ANN-based Clutter Reduction System Using its Best H, V, and R Integration Modes.

approach, improving the performances of the 1D modes by 4 dB, approximately. On the other hand, the performance improvement of the CA-based approach is practically constant to 1 dB, independently of the used integration mode. These objective results support the subjective analysis carried out previously. Moreover, note that the system performances achieved for this radar image are lower than the average values presented in Section 4.1 because it is the worst case found in the testing set. This selection has been done to show the high performance that can be achieved by the ANN-based clutter reduction systems, even working in difficult sea state and ship conditions.

4.3. Analysis of the Estimated Ship Sizes. An analysis of the estimated ship sizes in the CA-CFAR and ANN-based systems is presented. Figure 8 depicts a zoom of the most relevant area of the input and desired radar images depicted in Figure 3.

The same zoom is applied to the radar images at the output of the ANN-based clutter reduction system (Figure 4) and after thresholding (Figure 5), which are depicted in Figures 9 and 10, respectively. Different ship size estimations are obtained and depicted in Figure 10 depending on the used integration mode. The error in the length estimation of this ship (container ship) is 16 m (5.7%) using the horizontal

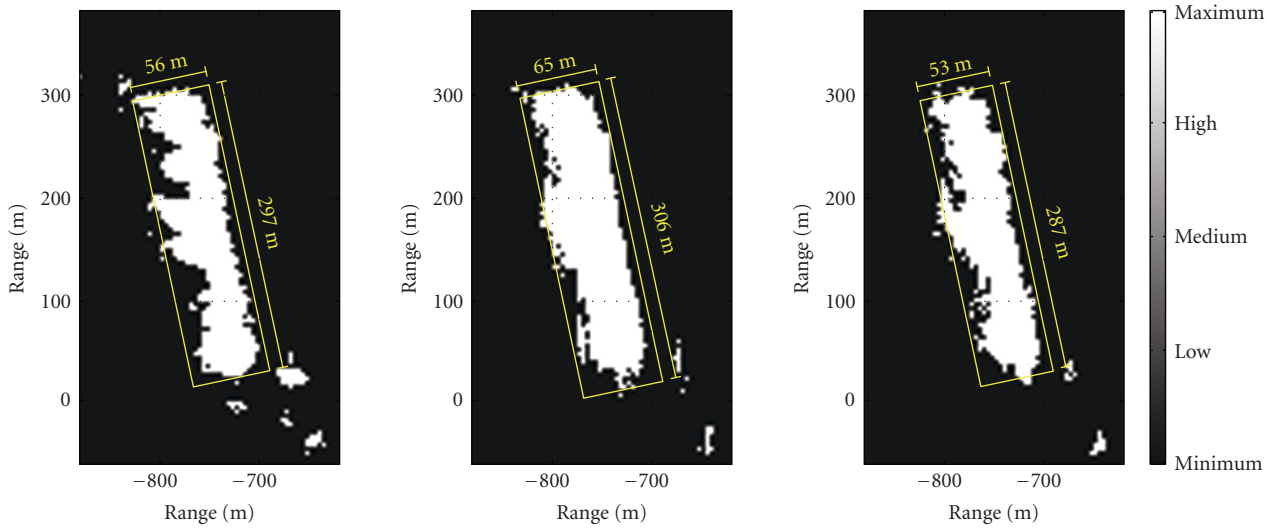

(a) Zoom of $\mathbf{O}^{\mathrm{H09,ANN\text{-}Det}}$ (b) Zoom of $\mathbf{O}^{\mathrm{V09,ANN\text{-}Det}}$ (c) Zoom of $\mathbf{O}^{\mathrm{R41,ANN\text{-}Det}}$

Figure 10: Zoom of the Images Processed by the ANN-based Detection System Using its Best H, V, and R Integration Modes.

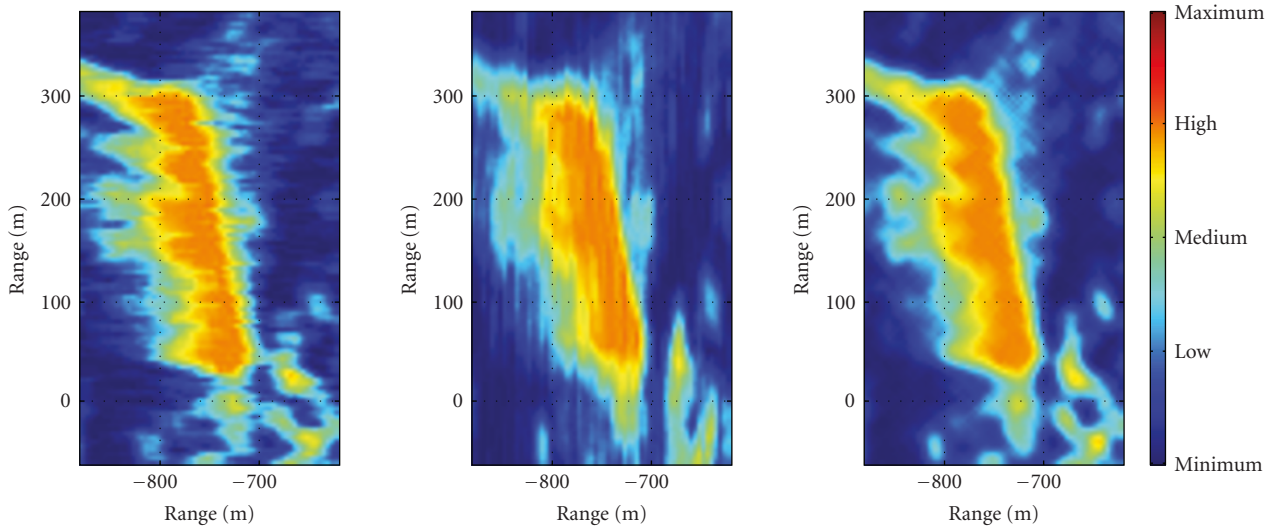

(a) Zoom of $\mathbf{O}^{\mathrm{H09,CA}}$ (b) Zoom of $\mathbf{O}^{\mathrm{V09,CA}}$ (c) Zoom of $\mathbf{O}^{\mathrm{R25,CA}}$

Figure 11: Zoom of the Images Processed by the CA System Using its Best H, V, and R Integration Modes.

integration mode, 25 m (8.8%) using the vertical integration mode and 6 m (2.1%) using the rhombus integration mode. The error in the width estimation of this ship is 25 m (80%) using the horizontal integration mode, 34 m (110%) using the vertical integration mode; and 22 m (70%) using the rhombus integration mode. As observed, accurate estimations of the length of this ship can be achieved, especially when the rhombus mode is used. This good behavior is due to the better clutter reduction and target enhancement achieved at the ANN output (see Figure 9). Nevertheless, in this radar image, poor ship width estimations are obtained, independently of the integration mode. It is important to remember that this radar image is the worst case of the testing set because of the huge electromagnetic ship diffraction. Substantially better results, in terms of ship size estimation, are obtained for the remaining radar images of the set. The average errors obtained in the estimation of the length and width of the different ships considered in the radar images of the testing set are, respectively, 6 m (2.1%) and 6 m (20%) using the horizontal integration mode, 9.5 m (3.3%) and 6 m (20%) using the vertical integration mode, and 3 m (1.1%) and 3 m (10%) using the rhombus integration mode.

Analyzing the results obtained with the CA-CFAR system, which are depicted in Figures 11 and 12, ship size estimation errors greater than the ones for the proposed ANN-based system are obtained, even for the rhombus integration

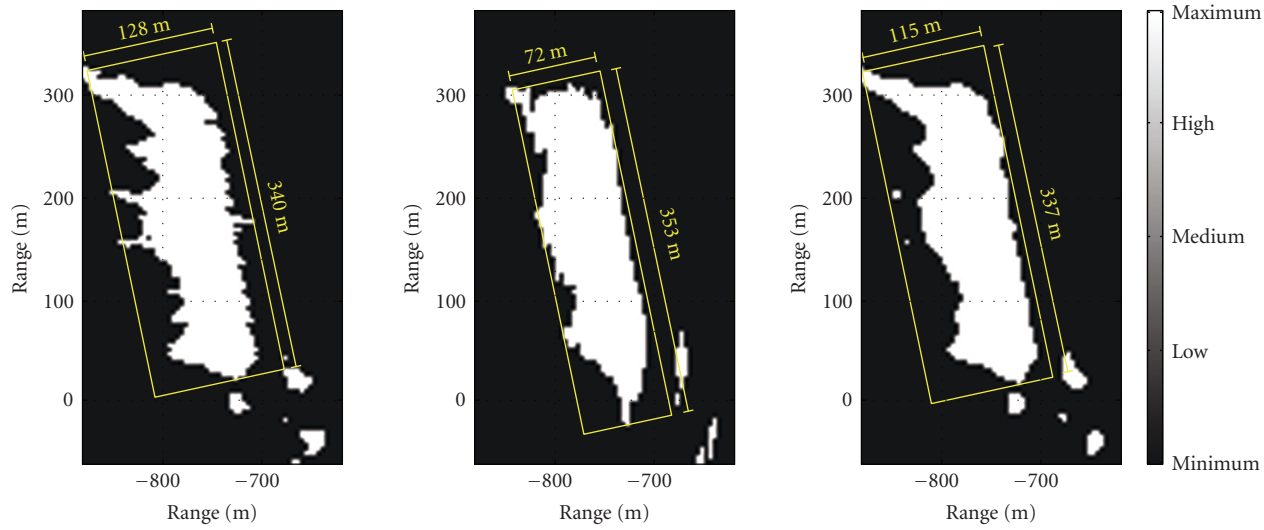

(a) Zoom of $\mathbf{O}^{\text{H09,CA-CFAR}}$ (b) Zoom of $\mathbf{O}^{\text{V09,CA-CFAR}}$ (c) Zoom of $\mathbf{O}^{\text{R25,CA-CFAR}}$

Figure 12: Zoom of the Images Processed by the CA-CFAR Detection System Using its Best H, V, and R Integration Modes.

mode. So, when using the CA-CFAR system, the average errors obtained in the estimation of the length and width of the different ships considered in the radar images of the testing set are, respectively, 18 m (6.3%) and 24 m (80%) using the horizontal integration mode, 28 m (9.8%), and 21 m (70%) using the vertical integration mode, and 15 m (5.6%) and 12 m (40%) using the rhombus integration mode.

5. Conclusions

A method for improving the estimation of the ship sizes in radar images obtained by maritime radars is proposed. The high estimation accuracy of this method is based on the better target enhancement and clutter reduction rates achieved by an efficient ANN-based clutter reduction system. Its high efficiency is achieved by the combination of horizontal and vertical information in a 2D (rhombus) shape at the input of the ANN. This 2D integration mode is able to improve by 5 dB the system performance (average SCR improvements of more than 17 dB) with respect to 1D modes (average SCR improvements of more than 12 dB).

Focusing on the ship size estimation, it is important to note that the system taken as reference, the CA-CFAR, presents poor ship size estimations, with minimum length and width average errors of 15 m (5.6%) and 12 m (40%), respectively. These problems are solved by the proposed ANN-based clutter reduction system followed by a fixed threshold, especially for the one that uses the 2D integration mode. In this case, accurate estimations of the length and width of a ship can be achieved, presenting average errors in their estimations of 3 m (1.1%) and 3 m (10%), respectively.

Apart of the performance improvements achieved by the different integration modes under study, a computational cost analysis is given. Although the computational cost of the ANN when using the rhombus mode is four times higher than the one needed when the 1D modes are used, this increase can be satisfied by the current FPGAs and DSPs working speeds. Anyway, if the system is computationally limited, the 1D modes can be used maintaining relatively high system performances, being always better than the ones achieved by the CA-CFAR system.

Finally, it is important to note that the proposed system presents great robustness in its performance against changes in sea clutter and ship conditions. Moreover, due to the mutual integration of vertical and horizontal information in the rhombus mode, this mode is able to work correctly and independently of the relative direction of movement of the ocean waves and ships with respect to the radar site. Moreover, although the proposed scheme is applied for a medium-range maritime radar, it could be also used in high-range radars, where ships can be located farther.

Acknowledgments

This research work has been supported by the *Ministerio de Educación y Ciencia* under Project no. TEC2009-14217 and by the *Comunidad de Madrid/Universidad de Alcalá* under Project no. CCG08-UAH/TIC-4242. The WaMoS II data obtained at the FINO 1 Platform was kindly provided by the *Federal Maritime and Hydrographic Agency of Germany* (Bundesamt fr Seeschiffahrt und Hydrographie, BSH) and OceanWaveS GmbH, Germany.

References

[1] A. Harati-Mokhtari, A. Wall, P. Brooks, and J. Wang, "Automatic identification system (AIS): data reliability and human error implications," *Journal of Navigation*, vol. 60, no. 3, pp. 373–389, 2007.

[2] G. Ellis and A. Dix, "A taxonomy of clutter reduction for information visualisation," *IEEE Transactions on Visualization and Computer Graphics*, vol. 13, no. 6, pp. 1216–1223, 2007.

[3] G. Ellis and A. Dix, "Enabling automatic clutter reduction in parallel coordinate plots," *IEEE Transactions on Visualization and Computer Graphics*, vol. 12, no. 5, pp. 717–723, 2006.

[4] D. Carevic, "Clutter reduction and target detection in ground penetrating radar data using wavelets," in *Detection and Remediation Technologies for Mines and Minelike Targets IV*, vol. 3710 of *Proceedings of SPIE*, pp. 973–978, Orlando, Fla, USA, April 1999.

[5] D. Carevic, "Clutter reduction and detection of minelike objects in ground penetrating radar data using wavelets," *Subsurface Sensing Technologies and Applications*, vol. 1, pp. 101–118, 2000.

[6] J. C. Nieto-Borge, K. Hessner, P. Jarabo-Amores, and D. de La Mata-Moya, "Signal-to-noise ratio analysis to estimate ocean wave heights from X-band marine radar image time series," *IET Radar, Sonar and Navigation*, vol. 2, no. 1, pp. 35–41, 2008.

[7] J. C. Nieto-Borge, A. M. Baquero-Martínez, D. de La Mata-Moya, and J. L. Álvarez-Pérez, "Analysis of the sea clutter structure using temporal sequences of X-band marine radar images," in *Proceedings of the International Conference on Radar (Radar '08)*, pp. 563–568, Adelaide, Australia, September 2008.

[8] J. C. Nieto-Borge, V. del Estal-Fernández, P. Jarabo-Amores, and K. Reichert, "Moving ship detection in presence of sea clutter from temporal sequences of marine radar images," in *Proceedings of the International Conference on Radar (Radar '08)*, pp. 88–93, Adelaide, Australia, September 2008.

[9] A. D. Van Merwe and I. J. Gupta, "A novel signal processing technique for clutter reduction in GPR measurements of small, shallow land mines," *IEEE Transactions on Geoscience and Remote Sensing*, vol. 38, no. 6, pp. 2627–2637, 2000.

[10] H. Brunzell, "Clutter reduction and object detection in surface penetrating radar," in *Proceedings of the Radar Edinburgh International Conference*, pp. 688–691, Edinburgh, UK, October 1997.

[11] B. Karlsen, H. B. D. Sorensen, J. Larsen, and K. B. Jakobsen, "Independent component analysis for clutter reduction in ground penetrating radar data," in *Detection and Remediation Technologies for Mines and Minelike Targets IV*, vol. 4742 of *Proceedings of SPIE*, pp. 378–389, Orlando, Fla, USA, April 2002.

[12] B. Karlsen, J. Larsen, H. B. D. Sorensen, and K. B. Jakobsen, "Comparison of PCA and ICA based clutter reduction in GPR systems for anti-personal landmine detection," in *Proceedings of the 11th IEEE Workshop on Statistical Signal Processing*, pp. 146–149, Singapore, August 2001.

[13] R. S. Raghavan, "Analysis of CA-CFAR processors for linear-law detection," *IEEE Transactions on Aerospace and Electronic Systems*, vol. 28, no. 3, pp. 661–665, 1992.

[14] S. Watts, "Performance of cell-averaging CFAR systems in sea clutter," in *Proceedings of IEEE National Radar Conference*, pp. 398–403, Alexandria, Va, USA, May 2000.

[15] S. Erfanian and V. Tabataba Vakili, "Introducing switching ordered statistic CFAR type I in different radar environments," *EURASIP Journal on Advances in Signal Processing*, vol. 2009, Article ID 525704, 11 pages, 2009.

[16] Z. Messali and F. Soltani, "Performance of distributed CFAR processors in pearson distributed clutter," *EURASIP Journal on Advances in Signal Processing*, vol. 2007, Article ID 21825, 7 pages, 2007.

[17] G. Hennessey, H. Leung, A. Drosopoulos, and P. C. Yip, "Sea-clutter modeling using a radial-basis-function neural network," *IEEE Journal of Oceanic Engineering*, vol. 26, no. 3, pp. 358–372, 2001.

[18] H. Leung, G. Hennessey, and A. Drosopoulos, "Signal detection using the radial basis function coupled map lattice," *IEEE Transactions on Neural Networks*, vol. 11, no. 5, pp. 1133–1151, 2000.

[19] M.-P. Jarabo-Amores, M. Rosa-Zurera, R. Gil-Pita, and F. Lopez-Ferreras, "Study of two error functions to approximate the Neyman-Pearson detector using supervised learning machines," *IEEE Transactions on Signal Processing*, vol. 57, no. 11, pp. 4175–4181, 2009.

[20] R. Vicen-Bueno, R. Carrasco-Álvarez, M. Rosa-Zurera, and J. C. Nieto-Borge, "Sea clutter reduction and target enhancement by neural networks in a marine radar system," *Sensors*, vol. 9, no. 3, pp. 1913–1936, 2009.

[21] R. Vicen-Bueno, R. Carrasco-Álvarez, M. Rosa-Zurera, and J. C. Nieto-Borge, "Sea clutter power reduction in radar measurement systems by feedforward multilayer perceptrons with medium input data integration rate," in *Proceedongs of IEEE Instrumentation and Measurement Technology Conference (I2MTC '09)*, pp. 1069–1075, Singapore, May 2009.

[22] F. Ziemer, C. Brockmann, R. Vaughan, J. Seemann, and C. Senet, "Radar survey of near shore bathymetry within the oroma project," *EARSeL eProceedings*, vol. 3, pp. 282–288, 2004.

[23] K. Reichert, K. Hessner, J. Dannenberg, I. Traenkmann, and B. Lund, "X-band radar as a tool to determine spectral and single wave properties," in *Proceedings of the 8th International Workshop on Wave Hindcasting and Forecasting*, 2005.

[24] World Meteorological Organization, http://www.wmo.int/pages/index_en.html.

[25] L. Gray, "A mathematician looks at wolfram's new kind of science," *Notices of the American Mathematical Society*, vol. 50, pp. 200–211, 2003.

[26] P. P. Gandhi and S. A. Kassam, "Analysis of CFAR processors in homogeneous background," *IEEE Transactions on Aerospace and Electronic Systems*, vol. 24, no. 4, pp. 427–445, 1988.

[27] C. Bishop, *Neural Networks for Pattern Recognition*, Oxford University Press, New York, NY, USA, 1995.

[28] S. Haykin, *Neural Networks. A Comprehensive Foundation*, Prentice-Hall, London, UK, 2nd edition, 1999.